Direct electron transfer of glucose oxidase and biosensing of glucose on hollow sphere-nanostructured conducting polymer/metal oxide composite

Chun Xian Guo and Chang Ming Li*

Received 28th April 2010, Accepted 14th June 2010
DOI: 10.1039/c0cp00378f

A hollow sphere-nanostructured conductive polymer/metal oxide composite was synthesized and used to investigate the electrochemical behavior of glucose oxidase, demonstrating a significantly enhanced direct electron transfer ability of glucose oxidase. In particular, the long-standing puzzle of whether enzymatic glucose sensing involves an enzyme direct electron transfer process was studied. The results indicate the mechanism is indeed a glucose oxidase direct electron transfer process with competitive glucose oxidation and oxygen reduction to detect glucose. A glucose biosensor with the glucose oxidase-immobilized nanomaterial was further constructed, demonstrating superior sensitivity and reliability, and providing great potential in clinical applications.

1. Introduction

Glucose oxidase (GOD) from *Aspergillus Niger* is a typical flavin enzyme with FAD (flavin adenine dinucleotide)/$FADH_2$ as the redox prosthetic group (active center).[1–3] It is known that the GOD molecule is a structurally rigid glycoprotein with a molecular weight of 152–186 kDa, and consists of two identical polypeptide chains, each containing a FAD redox center.[4–6] The biological function of GOD is to catalyze glucose to form gluconolactone. When GOD catalyzes glucose oxidation, the GOD-FAD is reduced to GOD-$FADH_2$, which can be oxidized by the electrode back to GOD-FAD with the following reactions:[7,8]

$$\text{GOD-FAD} + \text{glucose} \rightarrow \text{GOD-FADH}_2 + \text{gluconolactone} \quad (1)$$

$$\text{GOD-FADH}_2 \leftrightarrow \text{GOD-FAD} + 2\text{H}^+ + 2\text{e}^- \quad (2)$$

However, it is generally very difficult for GOD-$FADH_2$ to be directly oxidized electrochemically through the electrode reaction. The major barrier is that the active center FAD/$FADH_2$ is located at a depth of about 13 Å within the insulative apoenzyme, so even if the enzyme is tightly immobilized on the electrode surface, the distance between either one of its two FAD/$FADH_2$ centers and the electrode surface exceeds the critical electron tunneling distance.[3,9,10] Thus, the bioactivity of GOD is demonstrated by its ability to oxidize glucose through its FAD/$FADH_2$ redox center as shown in eqn (1). However, the insulative shell of GOD blocks the electron transfer between the FAD/$FADH_2$ redox center and the electrode surface as shown in eqn (2), resulting in poor electroactivity. To enable electron transfer between the active center of GOD and the electrode, traditionally, small diffusive electrochemical redox species called electron mediators are added to mediate the electron transfer, either in solution or immobilized on the electrode, and have been extensively used to fabricate glucose biosensors.[11–17]

With both theoretical significance and practical application due to their inherited simplicity, glucose biosensors based on direct electron transfer between the active center of GOD and the electrode have fueled extensive research efforts.[18–23] The use of nanostructured materials to facilitate direct electron transfer of GOD is one of the most popular approaches because they can immobilize GOD molecules to effectively shorten the electron tunneling distance by their superior quantum-confined physical, electronic and chemical properties.[24–29] Various nanomaterials reported such as graphene,[30] mesoporous TiO_2[31] and conducting polymer nanowires[32] with immobilized GOD have shown clear direct electron transfer of GOD and their glucose sensors have also been constructed with good performance. However, it remains a great challenge to develop new nanomaterials with even better direct electron transfer ability not only for use in sensitive enzymatic sensors, but also in biofuel cells with high energy conversion efficiency.[4,33,34] In addition, the contributions from both electrode and protein to the direct electron transfer of the enzyme are still not completely understood. In particular, it is a long-standing puzzle whether the mechanism of the glucose sensing is based on the direct electron transfer of GOD. The main argument is that direct electrochemistry based glucose sensors rely on the detection of decreased amperometric responses of oxygen reduction rather than directly sensing glucose oxidation. This is very similar to the early Clark glucose sensor which senses oxygen after consumption for H_2O_2 formation to determine glucose concentration,[12,35] but is not a direct electron transfer based sensor. Oxygen does not seem to function as an electron transfer mediator in these glucose sensors since all electron transfer mediator-assisted enzymatic sensors directly detect the glucose oxidation with a proportional response to the glucose concentration.[12,35]

In this study, a hollow sphere-nanostructured conducting polymer/metal oxide composite was synthesized and

Center for Advanced Bionanosystems and School of Chemical and Biomedical Engineering, Nanyang Technological University, 70 Nanyang Drive, Singapore 637457, Singapore. E-mail: Ecmli@ntu.edu.sg; Fax: +65 6791 1761; Tel: +65 6790 4485

characterized. The electrochemical properties, particularly the direct electron transfer behavior of GOD on the material were studied. A glucose biosensor based on GOD immobilized on the material was explored. Experiments were carefully designed and conducted to study the glucose sensing mechanism, and a possible mechanism was proposed.

2. Experimental details

2.1 Chemicals and materials

3,4-Ethylenedioxythiophene (EDOT) was purchased from Aldrich and vacuum distilled prior to use, and stored at 4 °C under protection of nitrogen. Glucose oxidase (*Aspergillus Niger*) was purchased from Sigma, and stored at −20 °C when not in use. All other chemicals were purchased from Sigma-Aldrich and used as received. If not specified, all solutions were prepared using deionized Millipore-Q water (18.1 MΩ cm).

2.2 Synthesis of hollow sphere-nanostructured conducting polymer/metal oxide composite

Carbon spheres were synthesized according a method reported previously.[36] Newly prepared carbon spheres were dispersed in water by ultrasonication to give a 0.5 wt% suspension. 20 mL of this suspension was added to 20 mL aqueous solution containing 0.01 M $NiCl_2$, 0.1 M urea, and 0.05 M sodium dodecyl sulfate and stirred further at room temperature for 10 min. The mixed solution was transferred into a 50 mL stainless steel autoclave and heated at 100 °C for 8 h. After it had cooled down naturally, the sample was taken out, rinsed with water and dried in a vacuum oven overnight. The dried sample was calcined at 650 °C for 3 h to produce NiO hollow spheres. For the formation of conducting polymer/NiO hollow spheres, EDOT was chosen because its polymerized form, PEDOT, has good stability and high conductivity.[37] Enough EDOT was added by micropipette to an aqueous solution containing 0.5 wt% hollow NiO spheres, and the mixture agitated for 10 min. After centrifuging, the precipitate was transferred to a vial and dried at 50 °C for 1 h, after which a solution of ammonium persulfate (0.1 M) was added. The mixture was stirred overnight for complete chemical polymerization to form poly(3,4-ethylenedioxythiophene) (PEDOT), which was isolated by centrifugation with water and ethanol washing, and dried at 50 °C overnight.

2.3 Preparation of enzyme electrodes

Prior to use, the glassy carbon electrodes (GCE, 3 mm in diameter) were polished to a mirror-like finish with 1.0, 0.3, and 0.05 μm alumina slurry followed by rinsing thoroughly with deionized water. The electrodes were successively sonicated in a 1 : 1 solution of nitric acid and acetone in doubly distilled water, and then allowed to dry at room temperature. Protein immobilization was achieved by immersing 20 mg of the as-prepared materials in 2 mL of GOD solution (10 mg mL^{-1}, pH 7.4, 0.01 M PBS (phosphate buffer solution)) under ambient conditions, which was shaken for 30 min and then stored at 4 °C overnight. The mixture was then centrifuged and 2 mL of pH 7.4, 0.01 M PBS was added for further use. The bioconjugates obtained were re-shaken and 5 μL of this suspension was deposited on the centre of the pretreated GCE, which was covered with an Eppendorf tube afterwards and dried overnight to prepare a uniform film. Finally, the modified GCE was thoroughly rinsed with water. When not in use, the electrode was stored in an aqueous solution of PBS (pH 7.4, 0.01 M) at 4 °C.

2.4 Material characterization and electrochemical measurements

The crystal structure of the materials was characterized by powder X-ray diffraction (XRD, Bruker AXS X-ray diffractometer). The morphology and microstructure were examined by field-emission scanning electron microscopy (SEM, JSM-6700F) and transmission electron microscopy (TEM, Hitachi 600). Nitrogen adsorption/desorption was carried out at 77.3 K by means of an Autosorb-1 analyzer. The protein secondary structure was examined by Fourier transform infrared spectroscopy (FTIR, Bruker EQUINOX 55 Duroscope™). Electrochemical measurements were performed using a CHI 760B electrochemical workstation (CH Instruments Inc.). The measurements were based on a three-electrode system with the as-prepared electrodes as the working electrode, a platinum wire as the auxiliary electrode, and a saturated calomel electrode (SCE) as the reference electrode. Although commercial sensors often use a two-electrode system (working-counter electrode) for low cost manufacturing, in electrochemical studies it is better to use a three-electrode system, which can have a well-defined polarization potential *versus* the reference electrode to investigate the electrode kinetics. For cyclic voltammogram tests, if not specified, all solutions were deoxygenated by bubbling highly pure nitrogen for at least 15 min and were maintained under a nitrogen atmosphere during the measurements.

3. Results and discussion

3.1 Material characterizations

The SEM image in Fig. 1a shows the template carbon spheres have an average diameter of 250 nm. After hydrothermal hydrolysis of the Ni^{2+} salt and heat-treatment in air to remove the carbon spheres, NiO hollow spheres (NiO HS) with an average diameter of 200 nm were obtained (Fig. 1b). The slightly smaller diameter of NiO HS in comparison with the carbon sphere template might be due to shrinkage during the high temperature treatment.[38] From the SEM image of two of the occasional broken NiO spheres (inset in Fig. 1b), it is obvious that the NiO wall is thin, with a thickness of ~15 nm. After deposition of conducting polymer PEDOT *via* intercalation[37] on NiO HS, the material (PEDOT-NiO HS) retains a spherical shape with an average diameter of 220 nm (Fig. 1c), indicating the thickness of PEDOT coated on NiO layer is ~10 nm. For the composite, the PEDOT loading on NiO HS is about 28% (w/w) based on thermogravimetric analysis. To gain more information about the structure of PEDOT-NiO HS, TEM was used. The strong contrast difference between the edge and the inside of these spheres (Fig. 1d) reveals that the sample consists of a hollow interior,

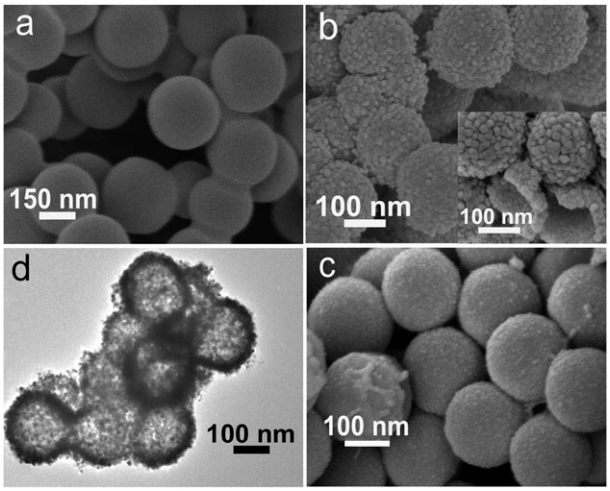

Fig. 1 SEM images of carbon spheres (a), NiO hollow spheres (HS) (b), and PEDOT-NiO HS (c). Inset of (b) shows two occasional broken NiO spheres. (d) TEM image of PEDOT-NiO HS.

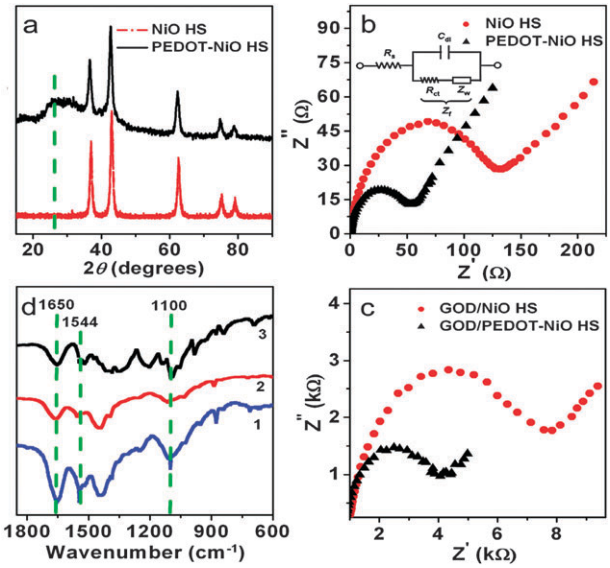

Fig. 2 (a) XRD patterns of NiO HS and PEDOT-NiO HS. Electrochemical impedance spectroscopy measurements in 1.0 M KCl containing 10 mM $Fe(CN)_6^{3-/4-}$ of electrodes before (b) and after (c) GOD immobilization. Inset of (b) is the Randle equivalent circuit. (d) FTIR spectra of plain GOD (1), GOD/NiO HS (2), and GOD/PEDOT-NiO HS (3).

which confirms that PEDOT-NiO HS is successfully fabricated.

To reveal the crystal structure and composition of the samples, XRD measurements were carried out. Fig. 2a shows the XRD pattern of NiO HS. According to the powder diffraction file, JCPDS 14-0117, all of the diffraction peaks can be readily indexed to the standard XRD values of NiO. After PEDOT deposition, apart from the peaks similar to that of NiO HS, there is a broad peak at $2\theta = 24.73^\circ$ ($d = 0.36$ nm), a typical XRD peak for PEDOT.[39,40] These results clearly show that the hollow spheres are composed of the metal oxide NiO and polymer PEDOT. The N_2 adsorption/desorption measurements indicate that the pore sizes of PEDOT-NiO are 5 to 20 nm with a large specific surface area of 234.2 $m^2\ g^{-1}$, which can be readily tailored to match the dimensional size of GOD (<8 nm)[31] for a large amount of GOD adsorption. The electrochemical properties were characterized by electrochemical impedance spectroscopy. The measured complex impedance (Z) *versus* frequency, known as a Nyquist plot, is shown in Fig. 2b. A Randle equivalent circuit (inset of Fig. 2b) is often used to model the complex impedance in an electrochemical cell, which is composed of the ohmic resistance of the electrolyte solution, R_s, in connection in series with parallel elements of double layer capacitance, C_{dl}, and Faraday impedance, Z_f. The parallel elements C_{dl} and Z_f *versus* frequency form a semicircle over a high frequency range, and Z_f often comprises serially connected charge transfer resistance, R_{ct}, which determines the diameter of the semicircle.[41] The values of R_{ct} that are calculated from the results in terms of the Randle equivalent circuit by using the software package ZSimpWin are 6.5 and 1.8 Ω cm^2 (surface area of GCE, 0.071 cm^2) for NiO HS and PEDOT-NiO HS electrodes, respectively, indicating that PEDOT-NiO HS has a much lower charge transfer resistance.

3.2 Protein immobilization and characterization

After GOD immobilization, the surface coverage of GOD on electrodes was calculated from the Nyquist plot shown in Fig. 2c. The charge transfer resistance of the hollow spheres after GOD immobilization, R_{ct}^{GOD}, is 689.5 and 299.2 Ω cm^2 for GOD/NiO HS and GOD/PEDOT-NiO HS electrodes, respectively, which is increased by a factor of ~100 compared with that (R_{ct}) obtained before GOD immobilization as shown in Fig. 2b. The surface coverage of GOD (θ) on the electrode can be derived from the equation $\theta = (1 - R_{ct}/R_{ct}^{GOD}) \times 100\%$.[42] The surface coverage of GOD confined on NiO HS and PEDOT-NiO HS electrodes is 99.3% and 99.4%, respectively, indicating that the surface coverage of GOD on PEDOT-NiO HS is comparable with that on NiO HS.

To better understand the protein conformational change after immobilization, the immobilized GOD on the samples was examined by FTIR, an efficient tool to study the bioactivity-related secondary structure of proteins. It is known that the amide I and II bands among the nine characteristic vibrational bands that arise from amide groups, together with the stretching vibration of the C–O bond, can provide the detailed secondary structure of proteins.[43] Two obvious IR absorption bands centered at 1650 and 1544 cm^{-1} are observed for GOD itself (curve 1 of Fig. 2d), ascribed to the typical amide I and II absorption bands, respectively. An absorption band around 1100 cm^{-1} is also seen, corresponding to the C–O stretching vibration of GOD. It is clear that the amide I band exhibits almost no change for GOD on both NiO HS (curve 2) and PEDOT-NiO HS (curve 3). On the other hand, the amide II band shows no change for GOD on PEDOT-NiO HS, whereas it is shifted by 15 cm^{-1} for GOD on NiO HS. Moreover, the stretching vibration band around 1100 cm^{-1} is still observed for GOD on PEDOT-NiO HS whereas it almost disappears for GOD on NiO HS. The FTIR results can provide solid evidence of whether GOD is probably denatured, or partially denatured after its immobilization.

Thus, the FTIR result here clearly indicates that GOD retains its native structure after its immobilization on PEDOT-NiO HS. It is very likely that the highly biocompatible PEDOT coating can prevent GOD from denaturing on the electrode as a result of immobilization.

3.3 Direct electron transfer studies

The electrochemical behavior of the different electrodes was studied by cyclic voltammograms (CVs). The plain GOD (curve a) and PEDOT-NiO HS (curve b) electrodes only exhibit typical capacitive CV responses caused by their double layer capacitance without any obvious redox peaks (Fig. 3), suggesting that both the GOD and PEDOT-NiO HS are electro-inactive over this potential window. For GOD/NiO HS electrode (curve c), there is a pair of weak redox peaks with anodic (E_{pa}) and cathodic (E_{pc}) peak potentials at −0.396 and −0.488 V (*vs.* SCE), respectively. The peak-to-peak separation (ΔE_p) and the formal potential (E°) are calculated as 92 mV and −0.442 V, respectively. The GOD/PEDOT-NiO HS electrode (curve d) shows a pair of well-defined redox peaks with E_{pa} and E_{pc} at −0.408 and −0.448 V (*vs.* SCE) respectively, corresponding to 40 mV for ΔE_p and −0.428 V for E°, respectively. The E° value of GOD on PEDOT-NiO HS is in accordance with the typical characteristics of GOD electrochemistry in neutral pH solution,[31] indicating that the redox center of GOD, FAD, is reduced to $FADH_2$ and reversibly reoxidized to FAD for a reversible redox process as shown in eqn (2). Based on Laviron's equation,[44] the heterogeneous electron transfer rate constant (k_s) can be calculated when the peak-to-peak separation is less than 200 mV. From curve d of Fig. 3, k_s of GOD on PEDOT-NiO HS is found to be 6.5 s^{-1}, much larger than that of GOD on NiO HS (3.12 s^{-1}, curve c of Fig. 3). The electroactive protein density (Γ^*, mol cm^{-2}) on the electrode surface can be estimated based on the formula $Q = nFA\Gamma^*$[21,30], where Q is the total charge passing through the electrode and A is the geometric area of the electrode, as 1.56×10^{-10} mol cm^{-2} for GOD/PEDOT-NiO HS, which is ten-fold higher than that of GOD/NiO HS (0.11×10^{-10} mol cm^{-2}). These results demonstrate the better direct electron transfer capability of GOD on PEDOT-NiO HS, which is consistent with the native structure of GOD on PEDOT-NiO HS shown in Fig. 2d.

As discussed above, the surface coverage of GOD on PEDOT-NiO HS (99.4%) is comparable with that of GOD on NiO HS (99.3%), thus the differences for k_s and Γ^* are not due to the relative amount of protein immobilized on the electrodes. It is known that GOD has an isoelectric point of 4.2 to carry negative charge in a neutral solution[9] and PEDOT has a certain amount of positive charges.[45] The electrostatic interaction between negatively charged GOD and positively charged PEDOT may push the active centers FAD/$FADH_2$ to access the electrode surface, thus shortening the tunneling distance for the fast direct electron transfer of the enzyme molecule. The FTIR studies show that GOD can hold its native structure on PEDOT-NiO HS, while it is probably denatured, or partially denatured on NiO HS. Moreover, the low charge transfer resistance of PEDOT-NiO HS from its low interfacial resistance (Fig. 2b) can also enhance the electron transfer from the enzyme redox centers to the bulk electrode.

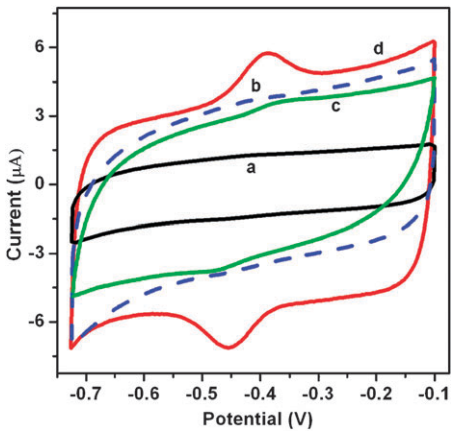

Fig. 3 Cyclic voltammograms (CVs) of the different electrodes in 0.1 M pH 7.0 nitrogen-saturated PBS solution at 100 mV s^{-1}. (a) Plain GOD, (b) PEDOT-NiO HS, (c) GOD/NiO HS and (d) GOD/PEDOT-NiO HS.

The effect of scan rate on the electrochemical response of GOD on PEDOT-NiO HS in Fig. 4a displays a linear relationship of redox peak current *versus* the scan rate, indicating that the GOD redox reaction is a surface-controlled electrochemical process from the FAD/$FADH_2$ active center of GOD on PEDOT-NiO HS.[31] The electrochemical response of GOD on PEDOT-NiO HS also shows a strong dependence on solution pH (Fig. 4b), in which the formal potential (E°) becomes more negative with increased solution pH, revealing that H^+ is involved in the electrochemical reaction of GOD. The slope of the peak potential (E_p) *versus* pH is 60.8 mV pH^{-1} (inset of Fig. 4b), which can be well explained by the redox reaction involved in the direct electrochemistry as shown in eqn (2). In terms of eqn (2), a theoretical value of 59.0 mV pH^{-1} for the slope of E° *versus* pH is expected, which is very close to the measured value of 60.8 mV pH^{-1}. Hence, the direct electron transfer reaction of GOD on PEDOT-NiO HS is a two-proton reaction coupled with a two-electron transfer process.[10,31,44] The pH value also affects the redox peak current of GOD (Fig. 4b), which increases as pH increases until the maximum peak current is reached around pH 7.0. With a further increase of pH, the peak current decreases, possibly indicating that the immobilized GOD has the highest bioactivity at pH 7.0.

3.4 Glucose oxidation and oxygen reduction on GOD/PEDOT-NiO HS

CV measurements with the GOD/PEDOT-NiO HS electrode were conducted in air-saturated PBS containing different concentrations of glucose, showing a prominent pair of redox peaks but with much higher cathodic peak current than the anodic one. The cathodic peak current achieves the highest value in air-saturated PBS without the presence of glucose (Fig. 5a). This apparently indicates that larger cathodic current is contributed by oxygen reduction. Interestingly, no obvious cathodic current is observed on the PEDOT-NiO HS electrode in air-saturated PBS (not shown), strongly proving

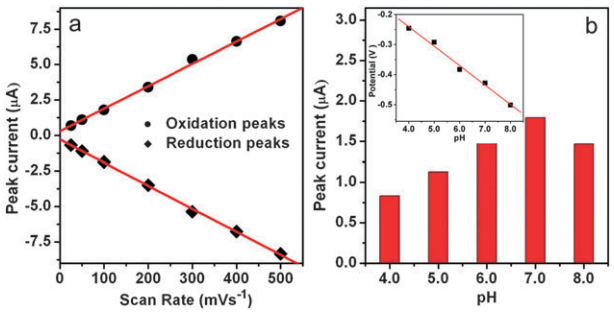

Fig. 4 (a) Plots of peak current *versus* scan rate from CVs of GOD/PEDOT-NiO HS (from 20 to 500 mV s^{-1}). (b) Plot of peak current *versus* pH value of GOD/PEDOT-NiO HS at 100 mV s^{-1}. Inset of (b) is the plot of E° *versus* pH value.

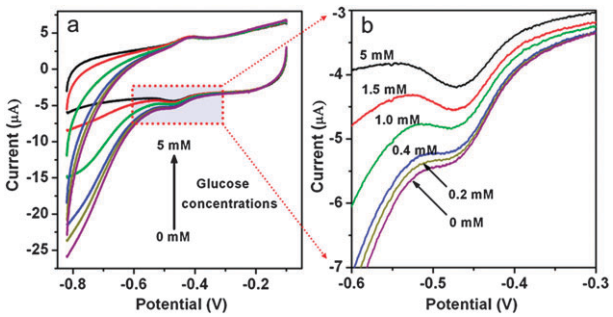

Fig. 5 (a) CVs of the GOD/PEDOT-NiO HS in air-saturated PBS solution with different concentrations of glucose. (b) The enlarged curves of the part shown in the rectangle of (a). Scan rate: 100 mV s^{-1}.

that GOD on PEDOT-NiO HS with direct electron transfer ability can significantly catalyze oxygen reduction. This is very different from the earliest Clark glucose sensor,[35,46] which uses a platinum electrode to measure the rate of oxygen uptake (eqn (4)) after consumption to form H_2O_2 under GOD catalysis (eqn (3)):

$$\text{glucose} + O_2 \rightarrow \text{gluconic acid} + H_2O_2 \quad (3)$$

$$O_2 + 4H^+ + 4e^- \rightarrow 2H_2O \quad (4)$$

Apparently, the Pt electrode in air-saturated solution without GOD load or the presence of glucose can measure the largest current from oxygen reduction. Thus the oxygen reduction on the GOD/PEDOT-NiO electrode is catalyzed by GOD, very likely through the direct electron transfer process of GOD as follows:

$$2\text{GOD-FADH}_2 + O_2 \rightarrow 2\text{GOD-FAD} + 2H_2O \quad (5)$$

for a 4-electron transfer path of oxygen reduction,[47] or

$$\text{GOD-FADH}_2 + O_2 \rightarrow \text{GOD-FAD} + H_2O_2 \quad (6)$$

for a 2-electron transfer path of oxygen reduction, followed by

$$\text{GOD-FADH}_2 + H_2O_2 \rightarrow \text{GOD-FAD} + 2H_2O \quad (7)$$

Followed by the redox reaction in eqn (2), in whichever case, the apparent net half cell reaction should be the same as eqn (4). Fig. 5 also presents another important fact, which is that the cathodic peak current in air-saturated PBS decreases with increasing the glucose concentration and can be used to determine glucose concentrations. This is very possibly ascribed to competitive glucose oxidation also occurring through GOD-FAD/GOD-$FADH_2$ reaction centers by the direct electron transfer path in terms of eqn (1) and (2).

To further confirm the competitive reactions of oxygen reduction and glucose oxidation through the direct electron transfer of GOD on PEDOT-NiO HS, CV measurements were conducted in nitrogen-saturated PBS containing different glucose concentrations. No anodic peak current was observed for PEDOT-NiO HS in the presence of glucose. For the GOD/PEDOT-NiO HS electrode in a solution without the presence of glucose, the anodic peak current is zero; upon addition of glucose, for increasing concentrations it increases accordingly (Fig. 6a). It can be found from the calibration curve in Fig. 6b obtained by subtracting the background that the anodic current linearly increases with increasing glucose concentration until it starts to saturate from 5 mM. This behavior is in good agreement with the enzymatic kinetic mechanism[17] and strongly supports the idea that glucose oxidation on the GOD/PEDOT-NiO HS electrode is based on the direct electron transfer of GOD. From the background-subtracted curves (Fig. 6b), around 0.4 μA anodic current increase results from 5 mM glucose added to nitrogen-saturated PBS, which is much lower than that of around 1.4 μA cathodic current decrease for 5 mM glucose addition in air-saturated PBS (Fig. 5b). This might be caused by the competitive adsorption of a much larger glucose molecule on the GOD/PEDOT-NiO HS surface that can block much smaller oxygen molecules from being absorbed, thus resulting in a larger decrease in current from oxygen reduction.

3.5 Glucose biosensor performance characterization

Because both *in vivo* and *in vitro* biological systems always contain oxygen, the decreased large cathodic current from competitive direct electron transfer reactions upon addition of glucose in air-saturated PBS can be used to detect glucose. The response of the GOD/PEDOT-NiO HS to successive injections of a glucose solution in air-saturated PBS at −0.45 V is shown in Fig. 7a (curve 2). Each addition of 0.18 μmol glucose results in a change in the steady state current with response time of less than 10 s. No obvious

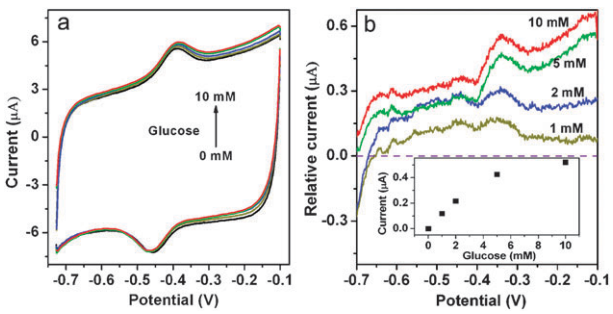

Fig. 6 (a) CVs of the GOD/PEDOT-NiO HS in nitrogen-saturated PBS solution with different concentrations of glucose. (b) Curves obtained by background-subtraction from (a) to eliminate charging current effect. Inset of (b) is the calibration curve. Scan rate: 100 mV s^{-1}.

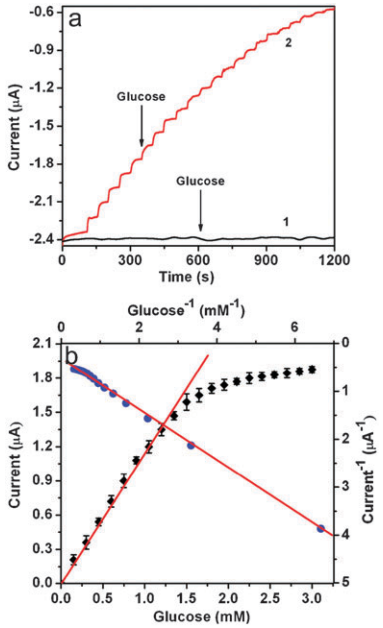

Fig. 7 (a) Current–time curves for successive additions of 0.18 μmol glucose to stirred pH 7.0, 0.1 M PBS at −0.45 V, (1) PEDOT-NiO HS and (2) GOD/PEDOT-NiO HS. (b) The calibration curve (current *versus* glucose concentration) and Lineweaver–Burk plot (current^{-1} *versus* concentration^{-1}) from curve 2 of (a).

response is obtained for the PEDOT-NiO HS electrode (curve 1), which is consistent with the above CV results.

The calibration plot in Fig. 7b obtained from curve 1 of Fig. 7a shows well defined, typical behavior of an enzymatic kinetic reaction with a linear regression equation of I_p (μA) = 1.2 (μA mM^{-1}) × C (mM) (n = 5, R = 0.989), where I_p is the peak current, C is glucose concentration, n is the number of electrodes measured and R is the correlation coefficient, in a range up to 1.5 mM, demonstrating a sensitivity of 16.9 μA mM^{-1} cm^{-2}, superior to that of glucose biosensors based on other nanomaterials (Table 1). When the glucose concentration is higher than 1.5 mM, a plateau current appears. The apparent Michaelis–Menten constant (K_M^{app}) gives an indication of the enzyme–substrate kinetics and a smaller value means a higher enzymatic activity and higher affinity towards the substrate. By using the electrochemical version of the Lineweaver–Burk equation,[12,48] $1/I_m = 1/I_{max} + K_M^{app}/(C \times I_{max})$, where I_m is the steady-state current, I_{max} is the maximum current, and C is the glucose concentration, a linear plot of $1/I_m$ *vs.* $1/C$ (Fig. 7b) is obtained to calculate K_M^{app} of GOD/PEDOT-NiO HS from its intercept and slope. A value of 1.82 mM is found, which is much smaller than 8.46 mM for the GOD/CNT electrode,[49] and 6.08 mM for a GOD/TiO_2 electrode.[50] The smaller K_M^{app} of GOD on PEDOT-NiO HS means that the enzyme electrode possesses higher enzymatic activity to glucose oxidation and higher affinity towards the substrate.

The stability of a biosensor is also critical. The GOD/PEDOT-NiO HS glucose sensor was tested by continuous CV measurements for 5 h and the amperometric response dropped by less than 2.5%. The enzyme electrode was stored at 4 °C when not in use. It could retain 95% of its initial amperometric response after storage for four weeks, which demonstrates that the sensor has good long-term life time and sustains a relatively long detection time (5 h) without significant drift.

Table 1 Comparison of sensitivity of various glucose sensors

Electrode material	Sensor sensitivity/ μA mM^{-1} cm^{-2}	Reference
GOD/PEDOT-NiO HS	16.9	This work
GOD/CNTs–silica	0.08	Ref. 19
GOD/Mesoporous TiO_2	3.9	Ref. 31
GOD/Nanocrystal TiO_2	4.6	Ref. 50
GOD/Porous carbon–silica	1.8	Ref. 43
GOD/Nitrogen-doped CNTs	13.0	Ref. 10

4. Conclusion

In summary, a unique hollow sphere-nanostructured PEDOT/NiO composite was synthesized and characterized. The electrochemical properties of GOD immobilized on the material were systematically investigated, demonstrating fast direct electron transfer resulting from the electrostatic interaction and retained conformation of GOD. In particular, the sensing mechanism of the glucose sensor based on the direct electron transfer of GOD on the material was studied. Results indicate that competitive reactions through the direct electron transfer path towards oxygen reduction and glucose oxidation result in a significantly decreased oxygen reduction current, allowing sensitive detection of glucose. A glucose sensor was constructed with the GOD immobilized material and exhibited high sensitivity and long term-stability. This work not only demonstrates a unique nanomaterial for enhanced direct electron transfer of GOD and its application in a high performance glucose sensor, but also provides fundamental insights to understand the direct electron transfer process, particularly the mechanism of the enzyme direct electrochemistry based glucose sensor.

Acknowledgements

This work was financially supported by the Center for Advanced Bionanosystems, Nanyang Technological University, Singapore.

References

1 O. Courjean, F. Gao and N. Mano, *Angew. Chem., Int. Ed.*, 2009, **48**, 5897.
2 S. B. Bankar, M. V. Bule, R. S. Singhal and L. Ananthanarayan, *Biotechnol. Adv.*, 2009, **27**, 489.
3 N. G. Tognalli, P. Scodeller, V. Flexer, R. Szamocki, A. Ricci, M. Tagliazucchi, E. J. Calvo and A. Fainstein, *Phys. Chem. Chem. Phys.*, 2009, **11**, 7412.
4 V. Coman, C. Vaz-Dominguez, R. Ludwig, W. Herreither, D. Haltrich, A. L. De Lacey, T. Ruzgas, L. Gorton and S. Shleev, *Phys. Chem. Chem. Phys.*, 2008, **10**, 6093.
5 T. Sugihara, H. Hotta and T. Osakai, *Phys. Chem. Chem. Phys.*, 2004, **6**, 3563.
6 O. Azzaroni, B. Yameen and W. Knoll, *Phys. Chem. Chem. Phys.*, 2008, **10**, 7031.
7 J. P. Liu, C. X. Guo, C. M. Li, Y. Y. Li, Q. B. Chi, X. T. Huang, L. Liao and T. Yu, *Electrochem. Commun.*, 2009, **11**, 202.
8 Y. Xiao, F. Patolsky, E. Katz, J. F. Hainfeld and I. Willner, *Science*, 2003, **299**, 1877.

9 D. Ivnitski, B. Branch, P. Atanassov and C. Apblett, *Electrochem. Commun.*, 2006, **8**, 1204.
10 S. Y. Deng, G. Q. Jian, J. P. Lei, Z. Hu and H. X. Ju, *Biosens. Bioelectron.*, 2009, **25**, 373.
11 Q. Lu and C. M. Li, *Biosens. Bioelectron.*, 2008, **24**, 767.
12 C. M. Li and C. S. Cha, *Front. Biosci.*, 2004, **9**, 3324.
13 A. Heller, *Phys. Chem. Chem. Phys.*, 2004, **6**, 209.
14 B. Brogioni, D. Biglino, A. Sinicropi, E. J. Reijerse, P. Giardina, G. Sannia, W. Lubitz, R. Basosia and R. Pogni, *Phys. Chem. Chem. Phys.*, 2008, **10**, 7284.
15 M. Chen and G. W. Diao, *Talanta*, 2009, **80**, 815.
16 J. F. Zang, C. M. Li, X. Q. Cui, J. X. Wang, X. W. Sun, H. Dong and C. Q. Sun, *Electroanalysis*, 2007, **19**, 1008.
17 X. Q. Cui, C. M. Li, J. F. Zang and S. C. Yu, *Biosens. Bioelectron.*, 2007, **22**, 3288.
18 S. Demin and E. A. H. Hall, *Bioelectrochemistry*, 2009, **76**, 19.
19 D. Ivnitski, K. Artyushkova, R. A. Rincon, P. Atanassov, H. R. Luckarift and G. R. Johnson, *Small*, 2008, **4**, 357.
20 K. J. Elliott, A. Harriman, L. Le Pleux, Y. Pellegrin, E. Blart, C. R. Mayer and F. Odobel, *Phys. Chem. Chem. Phys.*, 2009, **11**, 8767.
21 Z. Y. Wang, S. N. Liu, P. Wu and C. X. Cai, *Anal. Chem.*, 2009, **81**, 1638.
22 C. Y. Deng, J. H. Chen, X. L. Chen, C. H. Mao, L. H. Nie and S.Z. Yao, *Biosens. Bioelectron.*, 2008, **23**, 1272.
23 K. Kaminski, E. Kaminska, K. Adrjanowicz, Z. Wojnarowska, P. Wlodarczyk, K. Grzybowska, M. Dulski, R. Wrzalik and M. Paluch, *Phys. Chem. Chem. Phys.*, 2010, **12**, 723.
24 J. Zhang, M. Feng and H. Tachikawa, *Biosens. Bioelectron.*, 2007, **22**, 3036.
25 S. D. Minteer, B. Y. Liaw and M. J. Cooney, *Curr. Opin. Biotechnol.*, 2007, **18**, 228.
26 G. Z. Liu, M. N. Paddon-Row and J. J. Gooding, *Electrochem. Commun.*, 2007, **9**, 2218.
27 D. Chen, G. Wang and J. H. Li, *J. Phys. Chem. C*, 2007, **111**, 2351.
28 A. Kranich, H. Naumann, F. P. Molina-Heredia, H. J. Moore, T. R. Lee, S. Lecomte, M. A. de la Rosa, P. Hildebrandt and D. H. Murgida, *Phys. Chem. Chem. Phys.*, 2009, **11**, 7390.
29 Z. H. Dai, J. Ni, X. H. Huang, G. F. Lu and J. C. Bao, *Bioelectrochemistry*, 2007, **70**, 250.
30 C. S. Shan, H. F. Yang, J. F. Song, D. X. Han, A. Ivaska and L. Niu, *Anal. Chem.*, 2009, **81**, 2378.
31 S. J. Bao, C. M. Li, J. F. Zang, X. Q. Cui, Y. Qiao and J. Guo, *Adv. Funct. Mater.*, 2008, **18**, 591.
32 Y. Y. Horng, Y. K. Hsu, A. Ganguly, C. C. Chen, L. C. Chen and K. H. Chen, *Electrochem. Commun.*, 2009, **11**, 850.
33 C. X. Guo, F. P. Hu, X. W. Lou and C. M. Li, *J. Power Sources*, 2010, **195**, 4090.
34 W. Sun, C. X. Guo, Z. H. Zhu and C. M. Li, *Electrochem. Commun.*, 2009, **11**, 2105.
35 C. M. Li, H. Dong, X. D. Cao, J. H. T. Luong and X. J. Zhang, *Curr. Med. Chem.*, 2007, **14**, 937.
36 X. M. Sun and Y. D. Li, *Angew. Chem., Int. Ed.*, 2004, **43**, 597.
37 C. O. Wu, Y. C. Liu and S. S. Hsu, *Synth. Met.*, 1999, **102**, 1268.
38 X. W. Lou, L. A. Archer and Z. C. Yang, *Adv. Mater.*, 2008, **20**, 3987.
39 K. Singh, A. Ohlan, P. Saini and S. K. Dhawan, *Polym. Adv. Technol.*, 2008, **19**, 229.
40 F. Tran-Van, S. Garreau, G. Louarn, G. Froyer and C. Chevrot, *J. Mater. Chem.*, 2001, **11**, 1378.
41 C. X. Guo, F. P. Hu, C. M. Li and P. K. Shen, *Biosens. Bioelectron.*, 2008, **24**, 819.
42 H. Q. Liu, Y. Tian and Z. F. Deng, *Langmuir*, 2007, **23**, 9487.
43 S. Wu, H. X. Ju and Y. Liu, *Adv. Funct. Mater.*, 2007, **17**, 585.
44 C. X. Cai and J. Chen, *Anal. Biochem.*, 2004, **332**, 75.
45 A. Kros, W. F. M. van Hovell, N. Sommerdijk and R. J. M. Nolte, *Adv. Mater.*, 2001, **13**, 1555.
46 L. C. Clark and C. Lyons, *Ann. N. Y. Acad. Sci.*, 1962, **102**, 29.
47 Q. Zhou, C. M. Li, J. Li and J. T. Lu, *J. Phys. Chem. C*, 2008, **112**, 18578.
48 R. A. Kamin and G. S. Wilson, *Anal. Chem.*, 1980, **52**, 1198.
49 Y. Y. Wang, X. S. Wang, B. Y. Wu, Z. Zhao, F. Yin, S. Li, X. Qin and Q. Chen, *Sens. Actuators, B*, 2008, **130**, 809.
50 Q. W. Li, G. A. Luo, J. Feng, Q. Zhou, L. Zhang and Y. F. Zhu, *Electroanalysis*, 2001, **13**, 413.